Journal of Applied Polymer Science

# Homogenization of Natural Rubber Network Induced by Nanoclay

**Yijing Nie,[1,2] Liangliang Qu,[1] Guangsu Huang,[1] Xiaoan Wang,[1] Gengsheng Weng,[1] Jinrong Wu[1]**

[1]College of Polymer Science and Engineering, State Key Laboratory of Polymer Materials Engineering, Sichuan University, Chengdu 610065, People's Republic of China

[2]School of Materials Science and Engineering, Jiangsu University, 301 Xuefu Road, Zhenjiang 212013, People's Republic of China

Correspondence to: G. Huang (E-mail: guangsu-huang@hotmail.com)

**ABSTRACT:** Vulcanization gives birth to the nonuniformity of rubber network, the identification of which is the basis of improvement of performance of rubber products. We established a visco-hyperelastic constitutive equation to reveal the quantitative distribution of the inhomogeneous network phases according to a three-phase model. The cross-linked network was assumed to be composed of the cross-linking cluster, the low network chain density domain and the fluid-like mass. The incorporation of clay with high specific surface area induced the effective uniformity of network structure by decreasing the content of the cross-linking cluster and increasing that of the low network chain density domain. These structural variations were responsible for excellent mechanical properties and strong strain-induced crystallization ability probed by the *in situ* synchrotron wide-angle X-ray diffraction. © 2014 Wiley Periodicals, Inc. J. Appl. Polym. Sci. **2014**, *131*, 40324.

**KEYWORDS:** clay; elastomers; crosslinking; crystallization

Received 17 September 2013; accepted 17 December 2013
**DOI: 10.1002/app.40324**

## INTRODUCTION

Natural rubber (NR), one of the most traditional polymer materials, can not be replaced even nowadays. Since the discovery of vulcanization by sulfur in 1839 and reinforcement by carbon black (CB) in 1904,[1] NR has been used to manufacture a wide range of industrial products, such as automobile tires, vibration isolators and surgical gloves. These far-ranging applications and the superior properties such as outstanding tensile strength, good rebound elasticity, and excellent crack growth resistance, originate from the cross-linking of long chains and the strain-induced crystallization ability during deformation.[2]

Though the mechanism of vulcanization has not been fully elucidated, it is accepted that curing reactions give birth to a heterogeneous network structure of rubber, which largely influences physical properties.[3,4] However, it is a pity that the effect of the network inhomogeneity on mechanical properties is still unknown due to the difficulty of determining the quantitative distribution of the heterogeneous phases. In addition, some special phenomena in strain-induced crystallization were found with the help of *in-situ* synchrotron wide angle X-ray diffraction (WAXD).[5–10] For example, it was probed that the majority of rubber chains remained in isotropic coil state even at large strains and only a few percent of chains were oriented or crystallized during stretching.[5–8] This was a proof that the highly deformed and the unoriented amorphous chains coexisted. Toki et al. attributed it to the nonhomogeneous distribution of cross-linking points.[5] Tosaka further proposed a new network structure model for the thermodynamic description of strain-induced crystallization.[11] He assumed that the network chains in cross-linked rubber were a combination of the elastically effective and the fluid-like components.[11]

There were also some direct evidences about the nonuniformity of NR network structure.[4,12,13] Ikeda et al. detected the existence of a dense network domain with a characteristic length scale of 10–100 nm by using small-angle neutron scattering.[4] In the meantime, they put forward a two-phase network structure model, which can successfully explain some features of strain-induced crystallization in sulfur-cured NR.[4] Nevertheless, it should be noted that there are some inconsistencies among the three models mentioned above, which will be discussed in detail in the third part of our article. Moreover, due to fast progress in nanotechnology, the physical properties of NR can be enhanced by the inclusion of a small amount of nanosized particles.[14–18] Unfortunately, the reinforcement mechanism is still poorly understood.[19] Since structure determines property in material science, the effect of fillers on the microstructure of NR should be revealed before the full comprehension on the reinforcement mechanism and the large-scale using of nanocomposites. Saalwächter et al. have published many excellent

**Table I.** Formulations of the NR Composites

| Sample | NR phr[c] | OMMT phr | N330 Phr | Stearic acid Phr | ZnO Phr | Antioxidant 4020[a] Phr | Accelerator M[b] Phr | Sulfur phr | $t_{90}$ min |
|---|---|---|---|---|---|---|---|---|---|
| NR | 100 | - | - | 2 | 5 | 1 | 1 | 2 | 7.26 |
| NR/CB | 100 | - | 30 | 2 | 5 | 1 | 1 | 2 | 10.70 |
| NR/clay | 100 | 5 | - | 2 | 5 | 1 | 1 | 2 | 5.43 |

[a] *N*-(1,3-dimethylbutyl)-*N*′-phenyl-p-phenylene dianine.
[b] 2-Mercaptobenzothiazole.
[c] Parts by weight per hundred parts rubber (phr).

works about rubber–filler interactions and network characteristics by using NMR.[12,13,20,21] It was found that even exfoliated clay had obviously lower interactions with rubber matrix compared with conventional fillers, such as carbon black. Thus, the significantly enhanced mechanical properties were attributed to the filler networks.[20] The study of Carretero-González et al. showed that the addition of clay could provide a more homogeneous network structure.[19,22] Nevertheless, their results were preliminary and did not show enough information about the changes of the network structure. Thus, in the present article, we try to propose a new three-phase model of network structure and use it to develop a visco-hyperelastic constitutive model which can disclose the detailed distribution of the heterogeneous phases and their evolutions caused by the inclusion of different fillers. Because the mainly used measurement in the article is the stress–strain method, which is one of the most common measurements in rubber industry, our work could provide a convenient way to control the microscopic network structure and then improve the macroscopic mechanical properties of rubber in industrialized process.

## EXPERIMENTAL

### Materials

NR (ribbed smoked sheet, NO. 1) was purchased from Indonesia. NR latex (NR content was 60 wt %) was obtained from Chinese Academy of Tropical Sciences (P.R.C.). CB (N330) was purchased from China Rubber Group Carbon Black Research & Design Institute (P.R.C.). Sodium montmorillonite with cation-exchange capacity (CEC) of 90 mmol/100 g and an interlayer spacing of 1.53 nm was kindly supplied by Zhejiang Fenghong MMT Chemical Company (P.R.C.).

### Preparation of NR Composites

Sodium montmorillonite (50 g) was dispersed in hot water (1000 mL) under stirring. Octadecyl trimethyl ammonium chloride (25 g) was also dissolved in hot water (300 mL) and then poured into the clay-water solution with stirring for 2 h at 80°C. The organoclay obtained was washed and filtered, and subsequently dried under vacuum at 80°C for 12 h to remove the residual solvent. The organoclay was swelled in distilled water under stirring at 60°C for 1 h. Subsequently, NR latex was added to the suspension, followed by ultrasonication for 20 min. The NR/clay emulsion was demulsified by freezing afterward. Then the product was washed and heated at 60°C under vacuum overnight. The NR/clay compound was used as a masterbatch for preparing NR/clay nanocomposites.

For the CB filled NR, N330 was added into a laboratory two-roll mill after the plastication of NR without special treating. The recipes of the rubber composites are shown in Table I. The ingredients listed were mixed on the mill at room temperature. The mixed compounds were cured at 155°C in an electrically heated hydraulic press for their optimal cure time derived from curing curves.

### Measurements and Characterization

The curing process at 155°C was analyzed with a curemeter produced by Beijing Youshen Electronic Apparatus Factory (Beijing, People's Republic of China).

Tensile tests of dumbbell shaped samples according to the Chinese National Standard GB/T1040-92 were performed on an Instron-5567 material tester at room temperature at a rate of 50 mm/min. Since the tensile behaviors of rubber samples at fast strain rate (such as 500 mm/min) would deviate from the equilibrium state, the authors chose low strain rate (50 mm/min) to approach the quasi-equilibrium condition.

The method reported by Leblanc and Hardy[23] was employed to determine the amount of bound rubber. The amount of bound rubber in wt % of initial rubber content of the compound is given by the following equation:

$$\mathrm{Br}\,\% = [(m_0 - m_1)/m_0] \times 100 \quad (1)$$

where $m_0$ is the rubber content in the sample, $m_1$ is the rubber content extracted by toluene during 72 hours at room temperature.

TEM experiments were carried out on JEM 2010 transmission electron microscope (JEOL Co.) under an acceleration voltage of 200kV. The specimens for TEM observations were prepared using a Leica ultramicrotome under cryogenic conditions with a diamond knife.

Synchrotron WAXD experiments were performed under room temperature at U7B beam-line in the National Synchrotron Radiation Laboratory (NSRL), University of Science and Technology of China, Hefei, China. The wavelength was 0.154 nm. During deformation two-dimensional (2D) WAXD patterns were recorded in every 180 s by using Mar CCD 165 X-ray detector system. A homemade tensile machine was used to produce symmetric deformation at a drawing speed of

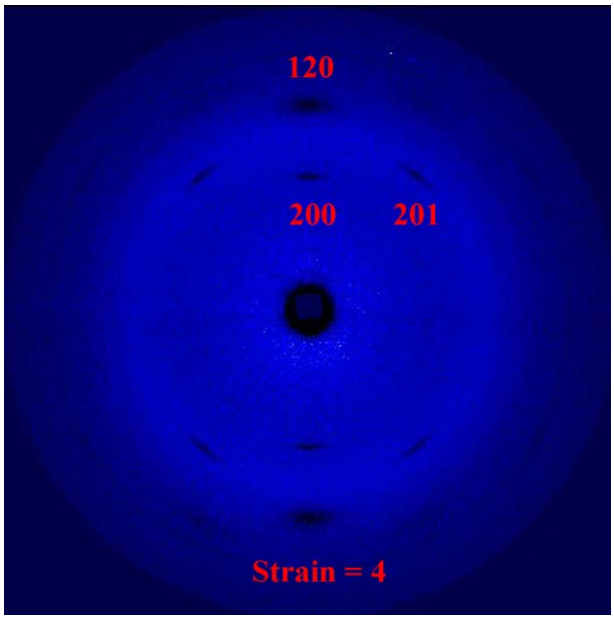


**Figure 1.** WAXD patterns of stretched pure NR at strain of 4. [Color figure can be viewed in the online issue, which is available at wileyonlinelibrary.com.]

4.2 mm/min, with the help of which the time-resolved WAXD patterns could be recorded continuously without holding the sample in still conditions. The strain $\varepsilon = (l - l0) / l0$ was determined from the distance between the clamps during deformation, in which $l0$ is the initial length of the sample and $l$ is the length of the elongated one. In the same way, the extension ratio ($\alpha$) was defined as $l/l0$. The Fit2D software package was used to analyze the 2D WAXD patterns. Air scattering was subtracted from all the WAXD patterns before quantitative analysis. The crystallinity index ($X_c$) was calculated from diffraction intensity data by using the following equation

$$X_c = \frac{\sum A_c}{\sum A_c + \sum A_a} \quad (2)$$

where $\sum A_c$ and $\sum A_a$ represent the corrected integrated intensities of the crystalline and amorphous regions, respectively.

## RESULTS AND DISCUSSION

### Different Features of Strain-Induced Crystallization

As shown in Figure 1, in addition to the highly oriented crystalline reflection peaks indexed as the 200, 120, and 201 reflections, the WAXD patterns of NR at high strains still possess the isotropic amorphous halo, indicating the coexistence of highly oriented chains and randomly coiled ones even in the highly stretched sample.[5–8,11] Figure 2 shows the variation of crystallinity as a function of strain for the three different rubbers. It can be found that crystallinity of the clay filled rubber is largest at same strain, while the unfilled NR has the lowest crystallinity. Meanwhile, according to the evolution of crystallinity during stretching, we can also obtain the onset strain of crystallization ($\varepsilon_0$), as listed in Table II. The clay filled NR has the lowest value of $\varepsilon_0$ (around 1) compared with the other two rubbers. The

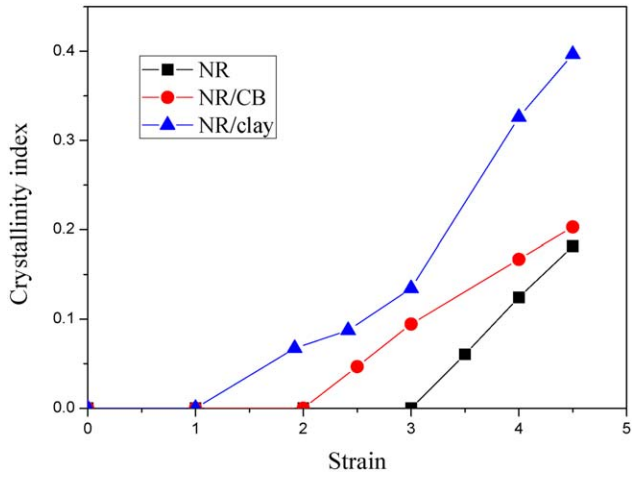


**Figure 2.** Evolution of crystallinity as a function of strain for different rubbers. [Color figure can be viewed in the online issue, which is available at wileyonlinelibrary.com.]

values of $\varepsilon_0$ for the CB filled and the unfilled rubbers are about 2 and 3, respectively.

The onset of crystallization is affected mainly by strain amplification.[2] In the study of CB filled rubber, Poompradub et al.[2] took into consideration that the effective strain of rubber matrix was larger than the nominal macroscopic one, because filler particles did not deform during deformation. For filled rubbers, $\varepsilon$, appropriate to rubber matrix can be replaced by the intrinsic strain of rubber portion in rubber composites, $\varepsilon'$ as follows[24]

$$\varepsilon' = \varepsilon\chi \quad (3)$$

where the amplification factor $\chi$ for describing the strain amplification effect of spherical fillers (CB) is expressed as[25]

$$\chi = 1 + 2.5\varphi + 14.1\varphi^2 = G/G_0 \quad (4)$$

while that reflecting the effect of non-spherical filler (clay) is given by[26]

$$\chi = 1 + 0.67 f\varphi + 1.62 f^2\varphi^2 = G/G_0 \quad (5)$$

where $\phi$ is the effective volume fraction of filler, $f$ is the shape factor, and $G$ and $G0$ are the initial moduli of the filled and unfilled rubber, respectively.

As shown in Table II, the modified intrinsic onset strain of crystallization of rubber portion in the clay filled rubber ($\varepsilon'_0$) is still smaller than that of the pure NR, while that in the CB filled NR is similar with that of the neat, indicating that different mechanism of filler effect on the rubber network structure and special strain amplification in clay filled rubber exist.

**Table II.** Onset Strain of Crystallization for the Unfilled and Filled NR

| | NR | NR/CB | NR/clay |
|---|---|---|---|
| $\varepsilon_0$ | 3.0 | 2.0 | 1.0 |
| $\varepsilon_0'$ | - | 2.9 | 1.6 |

**Table III.** Mechanical Properties of NR Composites

| | Tensile strength (MPa) | Elongation at break (%) | Bound rubber (%) |
|---|---|---|---|
| NR | 8.70 | 570 | 0 |
| NR/clay | 26.7 | 590 | 19.5 |
| NR/CB | 21.8 | 450 | 0 |

The mechanical property testing also showed some interesting features. As shown in Table III, the clay filled rubber shows more drastic improvements in tensile strength (26.7 MPa) compared with the CB filled NR (21.8 MPa) without sacrificing its extensibility. It implies that effects of those two fillers on the morphology of rubber network are different. The work of Saalwächter et al. revealed that conventional fillers (carbon black and silane-modified silica) and nanoclay had different reinforcement mechanisms.[20] The strong filler–rubber interactions played an important role in the reinforcement of rubber filled with conventional fillers, while the mechanical filler network was the major origin of the reinforcement behavior in rubber filled with nanoclay.[20]

### A Three-Phase Model

In order to explain the peculiar experimental features of strain-induced crystallization in sulfur-cured NR, Toki et al. assumed that network was composed of molecules with a broad distribution of chain lengths between network points.[5] Under stretching, the molecules of small chain length between the dense network points can be oriented and form crystallites, while the molecules of much longer chain length would remain in the random coil state.[5,6,8] This model can successfully interpret the existence of the isotropic halo in the WAXD patterns even in the high stretched sample, as shown in Figure 1. Furthermore, Tosaka proposed a two-component model to describe network structure and crystallization behavior of NR.[11] He concretely supposed that the network chains should be regarded as a combination of the elastically effective and the fluid-like components. However, on the basis of small-angle neutron scattering analysis of vulcanized rubbers, Ikeda et al. put forward another two-phase model to speculate the inhomogeneous network structure,[4] which had some differences from Toki's and Tosaka's models. In Toki's and Tosaka's models, strain-induced crystallization was assumed to take place in the domain with high network chain density, while the low network chain density domain was treated as an incompressible fluid.[11] However, Ikeda's model showed that crystallization occurred mostly in the rubbery matrix with low network chain density, while the high network chain density domains functioned like reinforcing fillers.[4]

During curing, sulfur is inclined to be present near the surface of zinc oxide particles.[27,28] Meanwhile, a "chelate-type" complex of Zn is generated on the surface and responsible for activation of sulfur during vulcanization.[28,29] Thus, the sulfur cross-linking reaction is active on the surface and around zinc oxide, resulting in the cross-linking cluster (i.e., the high network chain density domain near zinc oxide).[30] The corresponding network

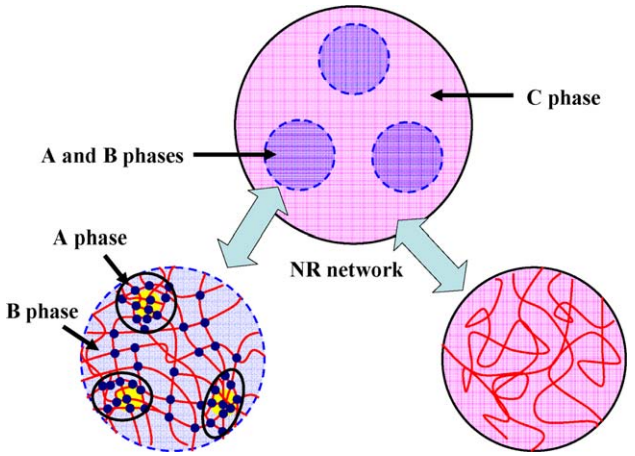


**Figure 3.** The inhomogeneous network structure of natural rubber. [Color figure can be viewed in the online issue, which is available at wileyonlinelibrary.com.]

chain density in the domain is so high that mobility, orientation and strain-induced crystallization of the rubber chains in the domain should be hindered by the large numbers of the cross-linking sites and the neighboring chains. Additionally, in the domain slightly away from zinc oxide, the network chain density is lower, and thus strain-induced crystallization can occur under stretching. In addition, due to the nonuniformity of curing, there are also some domains with the lowest network chain density far from zinc oxide, within which the rubber chains act as an incompressible fluid mass. According to the above analysis, we further propose a three-phase model to reveal the inhomogeneous network structure. As shown in Figure 3 (A,B) phases represent the high and the low network chain density domains, respectively, while C phase denotes the fluid-like component, which has very low network chain density or no cross-linking points.

### A Visco-Hyperelastic Constitutive Equation

According to the three-phase model proposed above, it can be deduced that during external loading besides hyperelastic responses resulting from A and B phases, there also exist continuous variations and accumulations of viscoelastic stress caused by C phase. Namely, the mechanical property of rubber is composed of the quasi-static hyperelastic behavior and the viscoelastic response.[31–33] Therefore, a reasonable and exact constitutive equation must contain both of these two contributions, which can be expressed as:[11]

$$\sigma = \phi_e \sigma_e + \phi_v \sigma_v \tag{6}$$

where $\sigma$ is the total nominal stress, $\sigma_e$ is the hyperelastic stress for unit mass of elastically effective phases (A and B phases), $\sigma_v$ is the viscoelastic stress for unit mass of C phase, $\phi_e$ and $\phi_v$ are the mass fractions of the elastically effective and the fluid-like parts, respectively. It should be noted that all of the stress used in the article is the nominal stress.

Owing to the very high network chain density, A phase acts as reinforcing filler for rubber.[30] Therefore, the hyperelastic stress mainly arises from B phase. In general, constitutive model for describing the hyperelastic stress can be established based on

the phenomenological theory and the statistic mechanics method.[34,35] Compared with the phenomenological approach, the statistic mechanics theory emphasizes much more on rubber chain conformation and network structure characteristic, which combines microstructural characteristic with macroscopic properties successfully.[35] In the statistic mechanics theory, there are two main approaches available in the description of the tensile stress–strain dependence in the low-elongation region: the Gaussian chain statistics theory and the tube model proposed by Edwards and his coworkers.[32–40] The former primarily pays attention to the impact of cross-linking points on network chain conformation and neglects the presence of a great deal of chain entanglements in rubber matrix. Actually, many experiments detected that the contribution of these topological entanglements to stress was significant and could not be ignored inconsiderately.[41,42] Hereby, in order to uncover real network structure more accurately, we choose the tube model as a reflection of hyperelasticity, which can properly separate the contributions of cross-linking and entanglement to the stress–strain behavior and determine the effect of entanglement on rubber elasticity.[43] The tube model takes into account the fact that topological constraints act along the whole chain, apply topological potential to every segments of the chain, and effectively restrict chain fluctuations to a virtual tube.[43,44] According to the ideas of Edwards et al., Heinrich et al. deduced the following stress–strain relations at uniaxial deformation, which consist of two contributions:[45,46]

$$\sigma_M=\sigma/\left(\alpha-\alpha^{-2}\right)=G_c+G_e f(\alpha) \tag{7}$$

$$f(\alpha)=\frac{2}{\beta}\frac{\alpha^{\beta/2}-\alpha^{-\beta}}{\alpha^2-\alpha^{-1}},f(\alpha=1)=1 \tag{8}$$

where $\sigma_M$ is the reduced stress, $\sigma$ denotes the nominal stress, $G_c$ is the elastic modulus resulting from the contribution of chemical cross-linking, $G_e$ is related to the topological tube-like constraints, $\beta$ is an empirical parameter describing the relation between the deformed tube in the stretched state and an undeformed tube corresponding to the equilibrium state. In general, $\beta$ is taken as 1.[45,46]

For the sake of keeping constitutive model simple and decreasing the amount of constants, we adopted a linear viscoelastic model to describe the viscoelastic behavior at small strains, which can be expressed as follows according to the Boltzmann superposition principle[47]

$$\sigma_v=\frac{\sigma_{vt}}{\alpha}=\frac{1}{\alpha}\int_0^t m(t-\tau)\dot{\varepsilon}d\tau \tag{9}$$

where $\sigma_{vt}$ is the true stress, $\varepsilon$ is strain, $\tau$ is time, $\dot{\varepsilon}=\partial\varepsilon/\partial\tau$ is strain rate, and $m(t)$ is the relaxation function

$$m(t)=\sum_{i=1-N}E_{vi}\exp\left(-t/\theta_i\right) \tag{10}$$

Where $\theta_i$ is the relaxation time, $N$ is the number of viscoelastic elements, and $E_{vi}$ is the modulus for unit mass of the elastically effective phases (A and B phases).

The mechanical response of many polymeric materials deformed at a wide range of strain rates generated by the Split Hopkinson Pressure Bar device could be adequately described by a single relaxation time.[31] In addition, a good model would not need a redundant number of parameters to describe the intrinsic features of the associated experimental phenomena. Accordingly, only one relaxation time is used herein, i.e., $N=1$ in eq. (10). Then, the following expression can be obtained

$$\sigma_v=\dot{\varepsilon}E_v\theta[1-\exp\left(-\varepsilon/\dot{\varepsilon}\theta\right)]/\alpha \tag{11}$$

In our visco-hyperelastic constitutive model, there are two kinds of elastically effective phases (A and B phases). Thus, $E_v$ should contain both contributions from the two phases

$$E_v=\phi_A G_A+\phi_B(G_c+G_e f(\alpha)) \tag{12}$$

where $\phi_A$ and $\phi_B$ are the mass fractions of A and B phases, respectively, $[G_c+G_e\,f(\alpha)]$ is the changing modulus of B phase depending on the strain due to the slippage of entanglements, and GA denotes the modulus of A phase. Finally, we attained the visco-hyperelastic constitutive equation

$$\begin{aligned}\sigma=&\phi_B(G_c+G_e f(\alpha))\ (\alpha-\alpha^{-2})\ +\phi_C(\phi_A G_A+\phi_B\\&(G_c+G_e f(\alpha)))\theta\dot{\varepsilon}\left(1-\exp\left(\frac{-\varepsilon}{\dot{\varepsilon}\theta}\right)\right)/\alpha\end{aligned} \tag{13}$$

where $\phi_C$ is the mass fraction of C phase. For filled NR, due to the strain amplification induced by filler, $\alpha$ according with rubber matrix should be replaced by the intrinsic extension ratio of rubber portion in rubber composites, $\alpha'$ as follows[24]

$$\alpha'=(\alpha-1)\chi+1 \tag{14}$$

where $\chi$ for describing the strain amplification effect of spherical fillers (CB) could be obtained according to eq. (4),[25] while that revealing the effect of non-spherical filler (clay) is given by eq. (5).[26]

**Effect of Fillers on Network Heterogeneity**

As shown in Table III, the inclusion of clay remarkably improves the tensile strength of NR without the sacrifice of its extensibility, while CB brings together the enhancement in the ultimate strength and the reduction in the extensibility. These phenomena imply that the effect of the two fillers on the rubber network structure should be different. In order to quantitatively elucidate the distribution of the network inhomogeneity and its evolution after the addition of fillers, the three-phase visco-hyperelastic constitutive equation was used to fit the stress–strain curves in the region of low elongation according to the least square fitting method by using origin 7.5 software, as displayed in Figure 4. The network structure parameters listed in Table IV can be obtained. Some heart-stirring results can be found. The uniformity of network structure could be related to changes in the structural parameters. The reduction of the content of A and C phases and the increasing of B phase would bring in more uniform network.

Firstly, the changes of distribution of the inhomogeneous network phases show different trends after the inclusion of the different fillers. The content of A phase decreases due to the presence of clay, while that in the CB filled NR increases

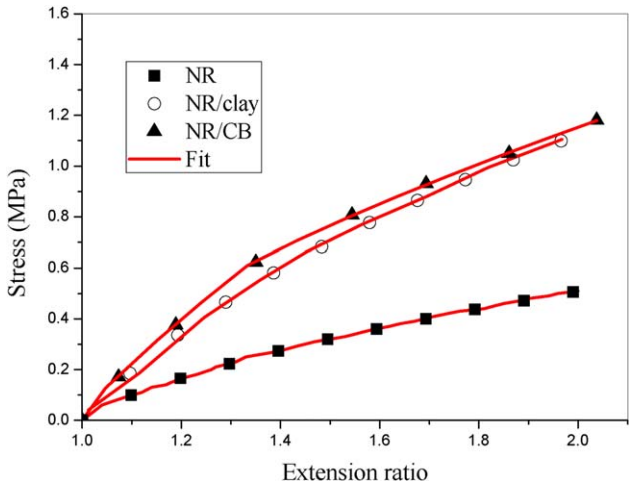


**Figure 4.** Fit results of stress–strain curves in the low-elongation region with the three-phase visco-hyperelastic constitutive equation. [Color figure can be viewed in the online issue, which is available at wileyonlinelibrary.com.]

compared with the neat NR. The content of B phase in the both filled rubbers increases in contrast with the neat rubber, but the incremental extent in the clay filled rubber is larger. Additionally, the content of C phase in the two filled rubbers drops after the inclusion of the two fillers. Secondly, the local network molecular parameters (*Gc* and *Ge*) of B phase also display some interesting variations. *Gc* increases by the inclusion of the two fillers, while *Ge* for the clay filled NR increases, presenting contrary trend compared with that for the CB filled NR. According to the evolutions of the parameters, it can be concluded that the addition of clay can induce the uniformity of network structure more effectively.[19] A schematic representation of the network structure evolutions by the addition of clay is shown in Figure 5.

For the clay filled rubber, there are two reasons for the uniform changes of the network structure. On the one hand, filler–rubber interactions were weak. As shown in Table III, no bound rubber was found in the clay filled rubber. The weak interactions between clay and rubber were detected recently by Saalwächter et al. by using NMR and equilibrium swelling measurements.[20] They found that even exfoliated clay particles did not significantly interact with the rubber matrix, and the reinforcement of clay filled rubber was attributed to the filler network.[20] The bound rubber caused by strong filler–rubber interactions would induced the heterogeneity of rubber network. In other words, the weak filler–rubber interactions and the absence of bound rubber contributed to the homogenization of rubber network. On the other hand, in the surface of clay, there

**Table IV.** Network Structure Parameters of the Unfilled and Filled Rubbers

| | $\phi_A$ | $\phi_B$ | $\phi_C$ | $G_A$ | $G_c$ | $G_e$ | $\theta$ |
|---|---|---|---|---|---|---|---|
| NR | 0.262 | 0.336 | 0.402 | 60.6 | 0.864 | 0.182 | 1.27 |
| NR/clay | 0.067 | 0.588 | 0.345 | 79.4 | 1.01 | 0.278 | 0.80 |
| NR/CB | 0.320 | 0.482 | 0.198 | 95.3 | 1.27 | 0.113 | 1.54 |

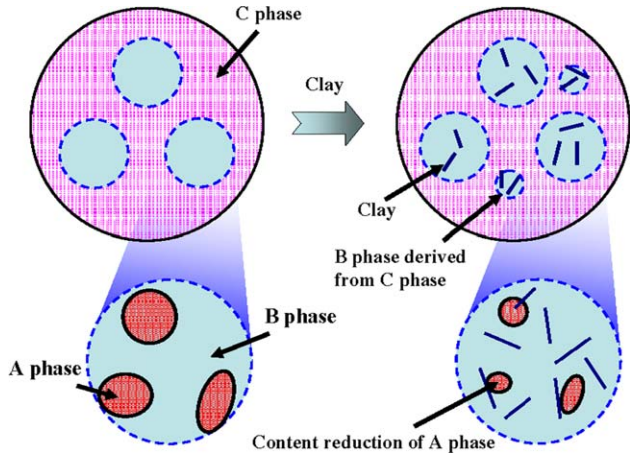


**Figure 5.** A schematic representation of the network structure evolutions by the addition of clay. [Color figure can be viewed in the online issue, which is available at wileyonlinelibrary.com.]

exist the ammonium groups of organic cations resulting from organo-modification, which would behave as effective accelerant agents for NR vulcanization.[15,48] Due to the high specific surface area of 700 $m^2/g$, the ammonium groups in the surface of exfoliated clay layers (Figure 6) have more chance to contact with rubber chains and sulfur. To validate the acceleration effect of the ammonium groups on NR vulcanization, curing curves for different rubbers were shown in Figure 7. It can be seen that the clay filled rubber had the fastest curing rate, as also revealed by the shortest optimum curing time ($t_{90}$) in Table I. Thus, the sulfur cross-linking reaction, which was formerly active on the surface and around zinc oxide,[29] can occur in the large-scale neighboring regions of clay and the cross-linking points would

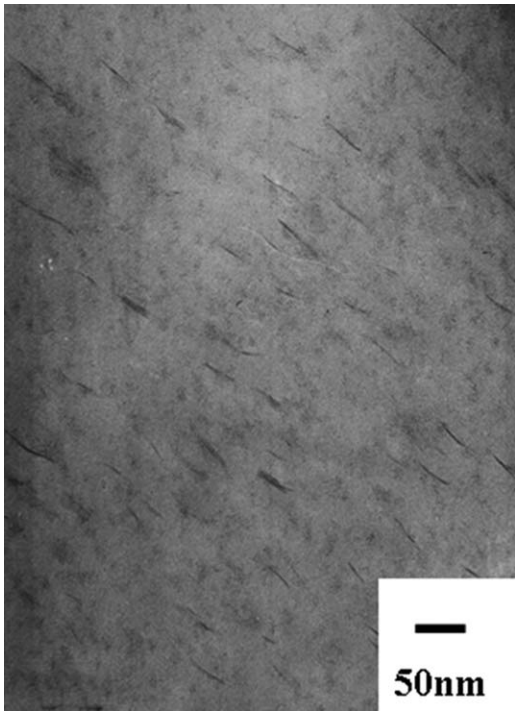


**Figure 6.** TEM micrographs of NR/clay nanocomposites.

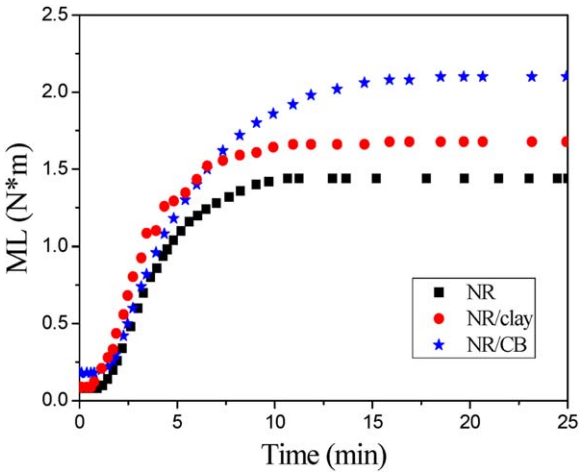


**Figure 7.** Curing curves for different rubbers. [Color figure can be viewed in the online issue, which is available at wileyonlinelibrary.com.]

distribute more homogeneously, leading to the evident reduction of $\phi_A$ and $\phi_C$, and the increment of $\phi_B$.

For the CB filled rubber, the existence of strong interactions between CB and rubber[20] can also induce limited uniform changes of network structure, as reflected by the increment of $\phi_B$ and the decreasing of $\phi_C$. Compared with clay, CB was inclined to fuse into large agglomerates in elastomer, and disperse on the microscale. Therefore, it has comparatively low specific surface area. Additionally, bound rubber can form around its particle surface,[45,49,50] resulting in the formation of both tightly and loosely absorbed rubber layers around the CB particles.[45] As listed in Table III, the fraction of bound rubber in the CB filled rubber was about 19.5%. The bound rubber could act as agglomerates of cross-linking domain, namely, giant cross-linking cluster. Thus, more A phase would come into being in or around the bound rubber. That is, the content of A phase in the CB filled rubber increases. This means that the increase of $\phi_B$ in the CB filled rubber derives from the decreasing of $\phi_C$, while that in the clay filled rubber mostly comes from the decreasing of $\phi_A$. The phenomenon can be also attributed to the existence of bound rubber. The dispersion of the bound rubber in the C phase can give birth to some effective cross-linking points, and thus changes some regions of C phase into B phase.

### Relationship Between Network Heterogeneity and Crystallization

According to the three-phase model, the mechanical properties are mainly determined by the microstructure in B phase, in which strain-induced crystallization takes place during deformation. In order to understand the structure-property relationship of NR, the tube model theory was applied further. Based on the model, Gc can be obtained by the expressions[51–53]

$$G_c = A_c \nu_c k_B T = \frac{A_c \nu_s l_s^2 k_B T}{\langle R_0^2 \rangle} \quad (15)$$

$$M_c = \rho_p N_A / \nu_c \quad (16)$$

where $\rho = 0.92$ g/cm$^3$ is the rubber density, $\nu_c$ is the network chain density, $\nu_s$ is the density of statistical segments, $N_A$ is Avogadro's number, $M_c$ is molecular mass of network chains, and $A_c$ is a microstructure factor that depends on the fluctuations of effective cross-linking junctions. According to the work of Klüppel, $A_c$ is equal to 0.67 in the case of moderately cross-linked network independent of cross-linking density.[53] $\langle R_0^2 \rangle = N l_s^2$ is the root-mean-square end-to-end distance between two successive junctions, $N = M_c/M_s$ is the mean number of statistical segments between successive junctions, $l_s$ is the average length of the Kuhn's statistical segment (0.76 nm for NR), and $M_s = 105$ g/mol is the molar mass of the statistical segments.[45,54] $G_e$ is correlated with the lateral dimension of the tube within the bulk rubber by the expression[45]

$$G_e = \frac{1}{4(6)^{1/2}} kT n_s \left(\frac{l_s}{d_0}\right)^2 \quad (17)$$

where $d_0$ is the fluctuation range of a chain segment (tube radius), $n_s = \rho N_A / M_s$ is the polymer segment number density taken as 5.46 nm$^{-3}$ in the article.[28] $d_0$ has a relationship with the mean number of statistical segments between successive entanglements ($n_e$) by the equation

$$d_0 = l_s n_e^{1/2} \quad (18)$$

Therefore, more local network molecular parameters disclosing the microstructure characteristics of B phase can be calculated. As listed in Table V, values of $d_0$ and $n_e$ decrease after the addition of clay, presenting different trends in comparison with the CB filled rubber. The reduction of tube dimension due to the presence of clay implies that the rubber chain movement has been restricted into a lower volume and the corresponding conformational entropy decreases.[16,55]

**Table V.** Local Network Molecular Parameters of B Phase

| | $\nu^*_c \times 10^4$ (mol cm$^{-3}$) | $M_c$ (g/mol) | $R_0$ (nm) | $N$ | $d_0$ (nm) | $n_e$ |
|---|---|---|---|---|---|---|
| NR | 3.19 | 1768 | 3.11 | 17 | 2.67 | 12 |
| NR/clay | 3.73 | 1485 | 2.84 | 14 | 2.16 | 8 |
| NR/CB | 4.69 | 1181 | 2.52 | 11 | 3.39 | 20 |

Some intriguing results were found in the strain-induced crystallization behaviors in the clay filled NR,[16,19,20] that is, the incorporation of clay brings on more remarkable promotion of strain-induced crystallization compared with the CB filled NR; the onset strain of strain-induced crystallization after modified by strain amplification is still smaller than that of crystallization in the neat NR,[16] differing from the phenomenon in the CB filled NR, whose onset strain of crystallization after modified by strain amplification is similar with that of the neat.[2,9] The underlying mechanism for these abnormal phenomena can be interpreted by the network structure evolution in B phase due to the incorporation of nanofiller. As shown in Table IV, $\phi_B$ in the clay filled NR is largest among the three kinds of rubbers, so the clay filled NR has the maximum content of the network chains which can crystallize under stretching, that is, it has strongest ability of strain-induced crystallization. This is also

one of the basic reasons for the dramatic reinforcing effect of clay on the mechanical property of NR. The network structure evolutions are also the reasons for maintenance of good extensibility after the addition of clay. In comparison with the neat NR, the clay filled NR has higher network chain density, which induces the reduction of extensibility. But in the meantime, it also has lower content of A phase, and thus reduces stress concentration regions, which is benefit for the improvement of extensibility. Thereby, the incorporation of clay does not lead to the decrease of extensibility. Contrarily, the inclusion of CB brings the rise of network chain density without the reduction of the content of A phase, so the maximum elongation decreases.

The onset of strain-induced crystallization is dominated by the entropy reduction ($\Delta S$), which is the entropy difference between the onset of crystallization and the unstretched (amorphous) states.[8,56,57] In general, $\Delta S$ is as a function of strain under the condition of uniaxial stretching according to the classical rubber elasticity theory[30]

$$\Delta S_0 = -(1/2)\nu_B k(\alpha_0{}^2 + 2/\alpha_0 - 3) \quad (19)$$

where $\alpha_0$ is the extension ratio when onset of crystallization occurs. In our previous article,[16] it was proposed that the entropy change of the clay filled rubber between the undeformed state and the onset of crystallization is composed of the entropy reduction caused by the addition of clay ($\Delta S_{01}$) and deformation ($\Delta S_{02}$), while that of the unfilled rubber is only caused by deformation ($\Delta S_0$). As demonstrated by the drop of the tube radius, the inclusion of clay with high specific surface area results in the emergence of a mass of rubber–filler interactions, leading to the enhancement of topology entanglements and packing effect, namely, the restriction of movement of rubber chains to a lower volume and the reduction of conformational entropy even without stretching ($\Delta S_{01}$). In conclusion, the special decrease of the onset strain of crystallization in the nanofiller filled NR should be attributed to $\Delta S_{01}$.

The analysis and results in the article reveal the quantitative distribution of the heterogeneous network structure, interpret the filler reinforcement mechanism from a new angle of view, and provide a new and convenient method to control and improve the physical properties of rubber materials.

## CONCLUSION

The heterogeneity of network structure in the cross-linked rubber can be estimated by the three-phase model, which assumes that the network is composed of the cross-linking cluster (A phase), the low network chain density domain (B phase), and the fluid-like mass (C phase). A phase acts as reinforcing filler in the rubber matrix, while B phase is responsible for the hyperelasticity, in which strain-induced crystallization can occur. In addition, C phase acts as a fluid mass, which provides the viscoelastic contribution. Based on the model, a visco-hyperelastic constitutive equation was established, which could quantitatively reveal the distribution of the inhomogeneous network phases.

We used the constitutive equation to study the network heterogeneity of NR and the evolutions after the inclusion of different fillers. The incorporation of clay induced the effective uniformity of network structure. Namely, $\phi_A$ decreased significantly, accompanied with the evident increase of $\phi_B$ and the reduction of $\phi_C$. The variations can be attributed to two reasons. Firstly, clay–rubber interactions were weak, and thus no bound rubber was formed in the clay filled rubber. Secondly, the ammonium groups in the surface of clay would behave as an accelerant agent for vulcanization, resulting in more uniform and much larger region for sulfur cross-linking reaction.

For the CB filled NR, $\phi_A$ increased due to the formation of bound rubber absorbed by the CB particles. Since the dispersion of the bound rubber in the C phase gave birth to some effective cross-linking points, $\phi_B$ increased with the reduction of $\phi_C$.

The structure-property relations can also be explained. The largest $\phi_B$ in the clay filled NR means that it has the maximum content of the network chains which can crystallize under deformation, that is, it has the best tensile strength. The maintenance of good extensibility can be attributed to the reduction of $\phi_A$. The special decrease of the onset strain of crystallization in the clay filled NR was due to $\Delta S_{01}$, which can be demonstrated by the decrease of the tube radius after the addition of clay. In a word, our work provides a new idea on the reinforcement of rubber.

## ACKNOWLEDGMENTS

This work was both kindly supported by the National Natural Science Foundation of China (NO.50673059 and 51333003) and the National Basic Research Program of China NO.2007CB714701. The authors also appreciate Professor Liangbin Li and Guoqiang Pan of National Synchrotron Radiation Laboratory (NSRL) in University of Science and Technology of China for the great help in Synchrotron WAXD experiments.

## REFERENCES

1. Yang, Q. Z. Modern Rubber Techniques; Sinopek press: Beijing, **2004**.
2. Poompradub, S.; Tosaka, M.; Kohjiya, S.; Ikeda, Y.; Toki, S.; Sics, I.; Hsiao, B. S. *J. Appl. Phys.* **2005**, *97*, 103529.
3. Shibayama, M. *Macromol. Chem. Phys.* **1998**, *199*, 1.
4. Ikeda, Y.; Higashitani, N.; Hijikata, K.; Kokubo, Y.; Morita, Y.; Shibayama, M.; Osaka, N.; Suzuki, T.; Endo, H.; Kohjiya, S. *Macromolecules* **2009**, *42*, 2741.
5. Toki, S.; Hsiao, B. S. *Macromolecules* **2003**, *36*, 5915.
6. Toki, S.; Sics, I.; Ran, S. F.; Liu, L. Z.; Hsiao, B. S.; Murakami, S.; Senoo, K.; Kohjiya S. *Macromolecules* **2002**, *35*, 6578.
7. Murakami, S.; Senoo, K.; Toki, S.; Kohjiya, S. *Polymer* **2002**, *43*, 2117.
8. Tosaka, M.; Murakami, S.; Poompradub, S.; Kohjiya, S.; Ikeda, Y.; Toki, S.; Sics, I.; Hsiao, B. S. *Macromolecules* **2004**, *37*, 3299.
9. Chenal, J. M.; Chazeau, L.; Guy, L.; Bomal, Y.; Gauthier, C. *Polymer* **2007**, *48*, 1042.

10. Trabelsi, S.; Albouy, P. A.; Rault, J. *Macromolecules* **2003**, *36*, 7624.
11. Tosaka, M. A. *Macromolecules* **2009**, *42*, 6166.
12. Valentín, J. L.; Posadas, P.; Fernández-Torres, A.; Malmierca, M. A.; González, L.; Chassé, W.; Saalwächter, K. *Macromolecules* **2010**, *43*, 4210.
13. Papon, A.; Saalwaüchter, K.; Schaüler, K.; Guy, L.; Lequeux, F.; Montes, H. *Macromolecules* **2011**, *44*, 913.
14. Joly, S.; Garnaud, G.; Ollitrault, R.; Bokobza, L.; Mark, J. E. *Chem. Mater.* **2002**, *14*, 4202.
15. Arroyo, M.; López-Manchado, M. A.; Herrero, B. *Polymer* **2003**, *44*, 2447.
16. Nie, Y. J.; Huang, G. S.; Qu, L. L.; Wang, X. A.; Weng, G. S.; Wu, J. R. *Polymer. 52*, 3234.
17. Nie, Y. J.; Huang, G. S.; Qu, L. L.; Zhang, P.; Weng, G. S.; Wu, J. R. *Polym. Adv. Technol.* **2011**, *22*, 2001.
18. Nie, Y. J.; Qu, L. L.; Huang, G. S.; Wang, B. Y.; Weng, G. S.; Wu, J. R. *Polym. Adv. Technol.* **2012**, *23*, 85.
19. Carretero-González, J.; Retsos, H.; Verdejo, R.; Toki, S.; Hsiao, B. S.; Giannelis, E. P.; López-Manchado, M. A. *Macromolecules* **2008**, *41*, 6763.
20. Valentín, J. L.; Mora-Barrantes, I.; Carretero-González, J.; López-Manchado, M. A.; Sotta, P.; Long, D. R.; Saalwächter, K. *Macromolecules* **2010**, *43*, 334.
21. Şerbescu, A.; Saalwaüchter, K. *Polymer* **2009**, *50*, 5434.
22. Carretero-González, J.; Verdejo, R.; Toki, S.; Hsiao, B. S.; Giannelis, E. P.; López-Manchado, M. A. *Macromolecules* **2008**, *41*, 2295.
23. Leblanc, J. L.; Hardy, P. *Kautsch. Gummi. Kunstst.* **1991**, *44*, 1119.
24. Eisele, U. Introduction to Polymer Physics, Springer-Verlag: Berlin, **1990**.
25. Guth, E.; Gold, O. *Phys. Rev.* **1938**, *53*, 322.
26. Guth, E. *J. Appl. Phys.* **1945**, *16*, 20.
27. Heideman, G.; Datta, R. N.; Noordermeer, J. W. M.; Van Baarle, B. *J. Appl. Polym. Sci.* **2005**, *95*, 1388.
28. Steudel, R.; Steudel, Y. *Chem. Eur. J.* **2006**, *12*, 8589.
29. Manik, S. P.; Banerjee, S. *Rubber Chem. Technol.* **1969**, *42*, 744.
30. Ikeda, Y.; Yasuda, Y.; Hijikata, K.; Tosaka, M.; Kohjiya, S. *Macromolecules* **2008**, *41*, 5876.
31. Shim, V. P. W.; Yang, L. M.; Lim, C. T.; Law, P. H. *J. Appl. Polym. Sci.* **2004**, *92*, 523.
32. Song, B.; Chen, W. N.; Cheng, M. *J. Appl. Polym. Sci.* **2004**, *92*, 1553.
33. Amin, A. F. M. S.; Lion, A.; Sekita, S.; Okui, Y. *Int. J. Plasticity* **2006**, *22*, 1610.
34. Meissner, B. *Polymer* **2000**, *41*, 7827.
35. Flory, P. *J. Chem. Rev.* **1944**, *35*, 51.
36. Kuhn, W. *Kolloid Z.* **1936**, *76*, 258.
37. Edwards, S. F. *Brit. Polym. J.* **1977**, *9*, 140.
38. Edwards, S. F.; Vilgis, T. A. *Rep. Prog. Phys.* **1988**, *51*, 243.
39. Doi, M.; Edwards, S. F. *J. Chem. Soc. Faraday Trans. 2* **1978**, *74*, 1789, 1802, 1818.
40. Doi, M.; Edwards, S. F. *J. Chem. Soc. Faraday Trans. 2* **1979**, *75*, 38.
41. Pearson, D. S.; Graessley, W. W. *Macromolecules* **1980**, *13*, 372.
42. Marrucci, G. *Macromolecules* **1981**, *14*, 434.
43. Doi, M. Introduction to Polymer Physics, Oxford University Press: Oxford, **1996**.
44. Rubinstein, M.; Panyukov, S. *Macromolecules* **1997**, *30*, 8036.
45. Heinrich, G.; Vilgis, T. A. *Macromolecules* **1993**, *26*, 1109.
46. Heinrich, G.; Kaliske, M. *Comp. Theor. Polym. Sci.* **1997**, *7*, 221.
47. Bower, D. I. An Introduction to Polymer Physics, Cambridge University Press: New York, **2002**.
48. Mousa, A.; Karger-Kocsis, J. *Macromol. Mater. Engng.* **2001**, *286*, 260.
49. Dannenberg, E. M. *Rubber Chem. Technol.* **1986**, *59*, 512.
50. Litvinov, V. M.; Steeman, P. A. M. *Macromolecules* **1999**, *32*, 8476.
51. Klüppel, M. *Macromolecules* **1994**, *27*, 7179.
52. Klüppel, M.; Schramm, J. *Macromol. Theory. Simul.* **2000**, *9*, 742.
53. Klüppel, M.; Heinrich, G. *Macromolecules* **1994**, *27*, 3596.
54. Aharoni, S. M. *Macromolecules* **1986**, *19*, 426.
55. López-Manchado, M. A.; Valentín, J. L.; Carretero, J.; Barroso, F.; Arroyo, M. *Eur. Polym. J.* **2007**, *43*, 4143.
56. Yamamoto, M.; White, J. L. *J. Polym. Sci. Part A-2* **1971**, *9*, 1399.
57. Nie, Y. J.; Gao, H. H.; Yu, M. H.; Hu, Z. M.; Reiter, G.; Hu, W. B. *Polymer* **2013**, *54*, 3402.